Journal of Materials Chemistry A

PAPER

View Article Online
View Journal | View Issue

Check for updates

Cite this: J. Mater. Chem. A, 2017, 5, 18527

Study of electronic interactions and photo-induced electron transfer dynamics in a metalloconjugated polymer–single-walled carbon nanotube hybrid by ultrafast transient absorption spectroscopy†

Haiting Shi,‡[a] Lili Du,‡[a] Wenjuan Xiong,[a] Mingjie Dai,[bc] Wai Kin Chan*[a] and David Lee Phillips*[a]

Received 30th March 2017
Accepted 8th August 2017

DOI: 10.1039/c7ta02753b

rsc.li/materials-a

Regioregular poly(thiophene) functionalized with pendant photosensitizing ruthenium complexes was synthesized. The conjugated polymer serves dual functions as a dispersant for single-walled carbon nanotubes (SWCNTs) and also as a photosensitizer. SWCNTs can be dispersed effectively by the polymer, and the polymer/SWCNT hybrid dispersion obtained was stable for months. Raman spectroscopic results showed that there was no structural damage or defects present in SWCNTs after the functionalization process and SWCNTs with both small (0.9 nm) and large (1.6 nm) diameter can be dispersed. Transmission electron microscopy revealed the presence of polymers on the SWCNT surface. The dynamics of the photo-induced electron transfer process between the ruthenium sensitizers and SWCNTs was probed by femtosecond transient absorption spectroscopy. Rapid electron injection from the ruthenium sensitizers to SWCNTs with a time constant of 167 ps was observed. By using this synthesis approach, it is possible to incorporate different types of sensitizers in one polymer chain so as to fine-tune the absorption spectra, and a new light harvesting system can be developed by coupling the polymer with SWCNTs.

Published on 17 August 2017. Downloaded by Rice University on 11/17/2023 5:06:50 PM.

Introduction

Single-walled carbon nanotubes (SWCNTs) have been demonstrated to be promising candidates for optoelectronic and photovoltaic devices because of their unique electronic and optical properties.[1–5] In this regard, the attachment of light-harvesting units as electron donors to CNTs and studies of the electronic interactions between these two moieties are at the forefront of investigations. It was reported that the photoexcitation involved a charge-transfer process from the sensitizer to carbon nanotubes, and photo-current was generated as a result of the sensitizer instead of SWCNT excitation. Metal complex sensitizers such as zinc porphyrin and phthalocyanine complexes have been used in CNT-based light harvesting systems because of their unique photophysical properties.[6–10] Photoinduced electron transfer processes between sensitizing CdS/CdTe/CdSe nanoparticles and carbon nanotubes were also reported.[11–13] Compared with small molecules, incorporation of the photosensitizers into polymer systems could produce a polymeric array with a combination of beneficial properties such as high optical cross-section and higher dispersing power for SWCNTs. It was reported that the properties of SWCNT-based electronic devices were dependent on the chirality and diameter of the nanotube, and sorted SWCNTs showed significant improvement in device performance.[14–16] Consequently, it is of great interest to develop polymer/SWCNT based light harvesting systems in which the nanotubes are sorted in the dispersion process. In addition, understanding the dynamics of the electron transfer process between the electron donor (sensitizer) and acceptor (SWCNTs) is also critical to the design of efficient light harvesting systems.

In this study, regioregular polythiophene functionalized with pendant ruthenium terpyridyl complexes was synthesized and the polymer was used as both sensitizer and dispersant for SWCNTs. The light harvesting metallopolymer was attached to the surface of the SWCNTs *via* non-covalent interactions, and could disperse the nanotubes effectively. The use of ruthenium polypyridyl complexes as sensitizers has been extensively

[a]Department of Chemistry, The University of Hong Kong, Hong Kong S. A. R., China. E-mail: waichan@hku.hku; Phillips@hku.hk

[b]Wyss Institute for Biologically Inspired Engineering, Harvard University, Boston, Massachusetts 02115, USA

[c]Department of Systems Biology, Harvard Medical School, Boston, Massachusetts 02115, USA

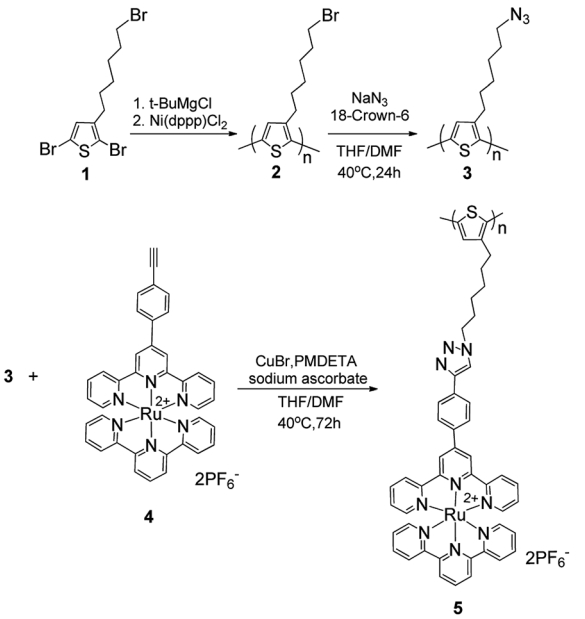
† Electronic supplementary information (ESI) available: Instrumentation and additional characterization data including NMR and FTIR spectra, molecular weight measurement results, TGA thermograms, EDX spectrum, and transient absorption spectra of complex **4** and polymer **2** are available. See DOI: 10.1039/c7ta02753b

‡ These co-authors contributed equally to this work.

Published on 17 August 2017. Downloaded by Rice University on 11/17/2023 5:06:50 PM.

studied.[17,18] These complexes were applied in artificial photosynthetic systems, dye-sensitized solar cells, and light sensors.[19,20] Polythiophene and its derivatives were demonstrated to be effective dispersants for SWCNTs. They are able to interact selectively with SWCNTs of specific chirality and diameter.[21,22] The polymer–SWCNT interactions are affected by the structure of the polymers such as the length and density of the pendant chain and main chain configuration.[23] Poly(3-alkylthiophene) with shorter pendant alkyl chains (*e.g.* hexyl group) could only disperse SWCNTs with smaller diameters (d < 1.2 nm)[22,24] but the dispersion effectiveness was low.[23] Attaching pendant ruthenium complexes to polythiophene not only introduces sensitizers onto the SWCNT surface but also improves the stability and solubility of the functionalized SWCNTs in polar solvents.

The incorporation of Ru(II) complexes to the polythiophene pendant chain was achieved by post-polymerization modification using a "click" reaction.[25] The metalloconjugated polymer obtained showed improved dispersibility for SWCNTs compared to unfunctionalized poly(3-alkylthiophene)s. Raman and TEM results showed that the polymer could disperse SWCNTs of various diameters. The Ru(II) complexes also play the role of photosensitizers, and the dynamics of the photoinduced charge separation processes in this donor–acceptor system were studied by femto-second transient absorption spectroscopy (fs-TA).



Scheme 1 Synthesis of side-chain functionalized poly(thiophene)s, polymer **5**.

Results and discussion

Synthesis of polymers

Poly(3-alkylthiophene)s can attach onto the SWCNT surface effectively *via* π–π interaction, and this process does not disrupt the optical and electronic properties of SWCNTs.[26] The synthesis of polymer **5** functionalized with pendant ruthenium complexes is shown in Scheme 1. Poly[3-(6-bromohexyl)thiophene] **2** was synthesized from the monomer 2,5-dibromo-3-(6-bromohexyl)thiophene **1** using Grignard metathesis polymerization, which was used in the synthesis of regioregular poly(3-alkylthiophene)s.[27] GPC results show that polymer **2** exhibits a number-average molecular weight M_n of 20 kDa with a polydispersity of 1.21. Reaction of **2** with sodium azide gave poly[3-(6-azidohexyl)thiophene] **3** in good yield (96%). By a simple click reaction with Ru(II) complex **4** that contains a terminal alkynyl group, target polymer **5** was obtained. Due to its chemical reactivity, polymer **3** was freshly prepared before undergoing the "click" reaction. The conversion from **2** to **3** was quantitative, as confirmed by ^{1}H spectroscopy (Fig. S1†). The peak at δ 3.44 ppm in polymer **2** is assigned to the CH_2 unit next to the bromide group. This peak shows an upfield shift to 3.29 ppm after the reaction with sodium azide, and no residual signal is observed at 3.44 ppm. After the click reaction, the ^{1}H NMR spectrum of polymer **5** (Fig. S1†) shows additional peaks at δ 7.15–8.99 ppm, which are assigned to the protons of the terpyridine ligand. In addition, the peak at δ 8.29 ppm is assigned to the protons on the triazole ring. The signal of the terminal methylene group next to the triazole ring showed a downfield shift to 4.31 ppm. The intensity of this peak is used to estimate the "click" conversion efficiency. It is estimated that 95% of the azide groups were attached with ruthenium complexes. The conversion from bromide to azide and then to ruthenium complexes is also confirmed by FTIR spectroscopy. Polymer **3** has an intense band at 2100 cm^{-1} (Fig. S2b†), which is assigned to the NN stretching of the azide group. After the click reaction, this stretching band is not observed in polymer **5** (see Fig. S2c†). In addition, compared with complex **4**, an additional intense absorption band due to the hexafluorophosphate P–F stretching is observed at 823 cm^{-1} (Fig. S2c and d†).

The UV-Vis absorption spectra of polymers **2**, **5**, and complex **4** are shown in Fig. 1a. Polymer **2** shows an intense absorption band centred at 440 nm assignable to the π–π* transition of the conjugated backbone.[28] Complex **4** exhibits two strong absorption bands centred at 311 and 489 nm, which are assigned to the ligand-centre (LC)[29] and metal-to-ligand charge transfer (MLCT) transitions of the Ru(II) complex.[30] For polymer **5**, the absorption bands due to the Ru(II) complexes can be clearly identified. On the other hand, the absorption due to the conjugated backbone only appears as a shoulder at *ca.* 430 nm. This is due to the very high Ru(II) complex content (close to one per thiophene unit), the absorption of which overwhelms the main chain absorption. It can also be seen that there is no significant shift in the absorption band positions between polymer **5** and polymer **2**/complex **4**, suggesting that the ground state electronic interaction between the polymer backbone and the Ru(II) complexes is not significant. Fig. 1b shows the emission spectra of polymers **2** and **5**. Polymer **2** shows an emission band centred at 580 nm due to the polythiophene main chain. However, in polymer **5**, the emission is almost completely quenched. This strongly suggests an energy transfer process between the excited state of the conjugated mainchain and the ruthenium complex

 This journal is © The Royal Society of Chemistry 2017

Published on 17 August 2017. Downloaded by Rice University on 11/17/2023 5:06:50 PM.

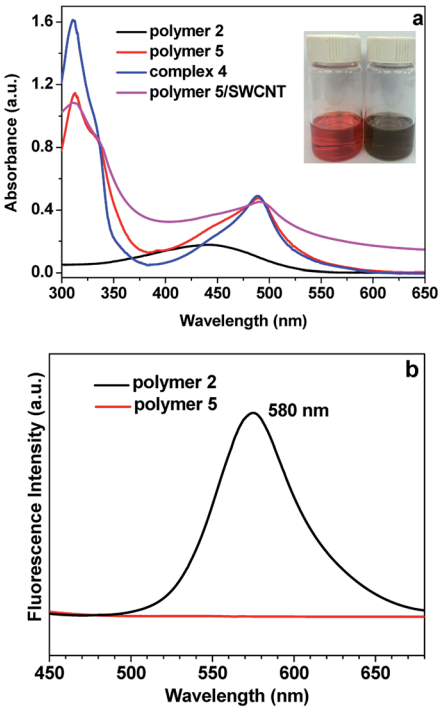


Fig. 1 (a) UV-Vis absorption spectra of polymer **2** (in $CHCl_3$) solution, complex **4**, polymer **5** (in DMF) solutions, and polymer **5**/SWCNT hybrid dispersion (in DMF). The inset figure shows polymer **5** solution (left) and polymer **5**/SWCNT dispersion (right). (b) Steady state fluorescence spectra of polymer **2** (in $CHCl_3$) and polymer **5** (in DMF). Excitation wavelength = 400 nm.

moieties, owing to an overlap between the polymer backbone emission and the Ru(II) complex absorption.[25]

The electrochemical properties of polymer **5** were studied by cyclic voltammetry (CV). As shown in Fig. S3,† the irreversible anodic waves at 0.15 V, reversible anodic wave at 0.9 V, and cathodic wave at −1.6 V are due to the oxidation of the backbone,[31] $Ru^{II/III}$ couple, and reduction of the terpyridine ligand, respectively. By comparing these potentials with a ferrocene internal standard,[32] the HOMO–LUMO levels of photosensitizer ruthenium complexes were calculated to be −5.7 and −3.2 eV, respectively. It was reported that SWCNTs have a narrow band gap of approximately 1 eV, and the work function of SWCNTs is around −4.47 eV.[33] The work function of SWCNTs having diameters larger than 1 nm shows no significant chirality or diameter dependence. Based on the electrochemical data, an energy level diagram showing the relative HOMO and LUMO levels of the sensitizing ruthenium complex with respect to those of SWCNTs is shown in Fig. 2. The band gap of SWCNTs (energy level of SWCNTs is referenced[33]) positions between the HOMO and LUMO levels of the Ru(II) complex. When the Ru(II) complex is excited, energy or electron/hole transfer from the Ru(II) to SWCNTs could occur because such processes are energetically favourable. For energy transfer, since the Ru(II) terpyridine complex is known to exhibit a very low emission quantum yield, the energy transfer from Ru(II) to SWCNTs will not be significant.

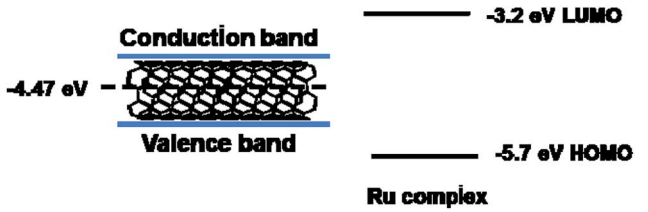


Fig. 2 Energy diagram of the HOMO and LUMO levels for the Ru complex and SWCNTs. The energy scale is given with respect to the vacuum level.

Preparation of the polymer/SWCNT hybrid

It was observed that polymer **2** was not able to disperse SWCNTs, while polymer **5** is an effective dispersant for SWCNTs in polar solvents. The homogeneous hybrid dispersion obtained was stable for more than three months. After the formation of the polymer **5**/SWCNT hybrid, there is a significant change in the appearance of the dispersion when compared to the pure polymer (Fig. 1a). In the UV-Vis absorption spectrum of polymer **5**/SWCNT hybrid dispersion (Fig. 1a), the very broad absorption band in the visible region is due to SWCNTs. As a result, the absorption due to the π-conjugated main chain is masked. Nevertheless, the absorption bands due to the LC and MLCT transitions of the Ru(II) complex can still be identified, which confirms the presence of polymer **5** in the hybrid.

The interaction between polymer **5** and SWCNTs was further examined by micro-Raman spectroscopy. Fig. 3 shows the Raman spectra of the polymer **5**/SWCNT hybrid and pristine SWCNTs. The characteristic bands due to the radial breathing mode (RBM), disorder mode (D band), and tangential vibrational mode (G band)[34] for pristine SWCNTs are observed at 134–261, 1295, and 1590 cm^{-1}, respectively. The D-bands observed in these two spectra remain unchanged after normalizing the intensities of the G-band, which suggests that

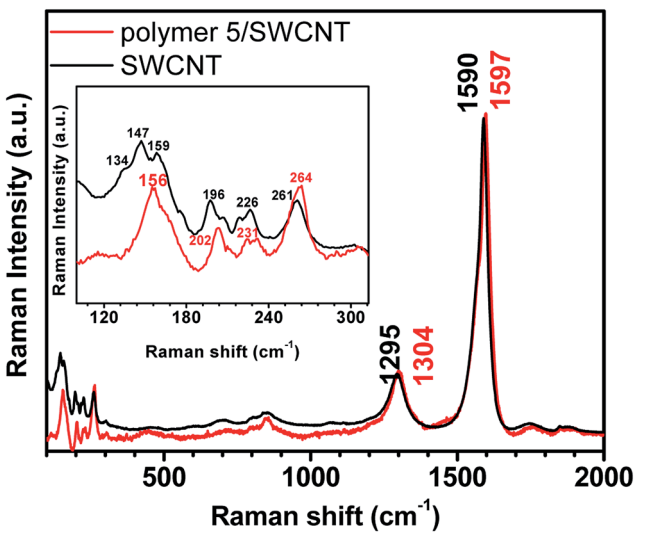


Fig. 3 Micro-Raman spectra of pristine SWCNTs and the polymer **5**/SWCNT hybrid (excited at 785 nm).

Published on 17 August 2017. Downloaded by Rice University on 11/17/2023 5:06:50 PM.

there is no structural damage or defects present in SWCNTs after functionalization.[22] After formation of the hybrid, both D, G, and RBM bands show a shift to a higher frequency, from 1295 to 1304 cm^{-1}, 1590 to 1597 cm^{-1}, and 134–261 to 156–264 cm^{-1}, respectively. It was reported that for SWCNTs, the shift of the G and RBM bands to a higher frequency indicated an electronic interaction between the dispersant and SWCNTs.[35,36] The diameter of SWCNTs can be estimated from the position of the RBM bands observed at 100–400 cm^{-1} by using the equation:

$$\omega_{RBM} = 223.5\ cm^{-1}/d + 12.5\ cm^{-1}$$

where ω_{RBM} is the frequency of the RBM band (in cm^{-1}), and d is the diameter of the SWCNTs (in nm).[37] For pristine SWCNTs, the diameter is in the range between 0.9 and 1.8 nm (RBM band frequency 261 to 134 cm^{-1}).[38] It can be seen that there are changes in the relative intensity of the RBM bands after the formation of the polymer/SWCNT hybrid. The intensities of the RBM bands at 264 and 156 cm^{-1} increased compared to those of pristine SWCNTs (Fig. 3), which suggests that polymer **5** has a more favourable interaction with SWCNTs with diameters of *ca.* 0.9 nm and 1.6 nm.[22] The diameter dependence indicates that the dispersed SWCNTs have narrower distribution of diameter and possess a better quality than raw SWCNTs in terms of structural homogeneity.[39]

The morphology of the polymer **5**/SWCNT hybrid was examined by transmission electron microscopy (TEM) and the images are shown Fig. 4 and S4.† It can be seen that both individual nanotubes as well as small bundles can be found in the mixture (Fig. S4†). Polymer **5** is able to exfoliate SWCNTs with very small diameters. High magnification TEM images of individual SWCNTs functionalized with polymer **5** are shown in Fig. 4a–d. A layer of polymer on the SWCNT surface can be identified. Fig. 4a and b show an isolated tube coated with polymer **5**. The diameter of the SWCNTs was measured to be 1 nm, which is consistent with the results obtained from Raman spectroscopy.

Fig. 4c and d show the TEM images of the polymer **5**/SWCNT hybrid in which the SWCNTs have a large diameter (~1.5 to 2 nm). EDX experiments confirmed the presence of Ru in the hybrids, which further supports the functionalization of SWCNTs by polymer **5** (Fig. S5†). Scheme 2 shows the schematic representation of a SWCNT functionalized with polymer **5**. The conjugated main chains interact with SWCNTs *via* π–π stacking, which facilitates the electron transfer process between the Ru(II) complex sensitizers on polymer **5** and SWCNTs.

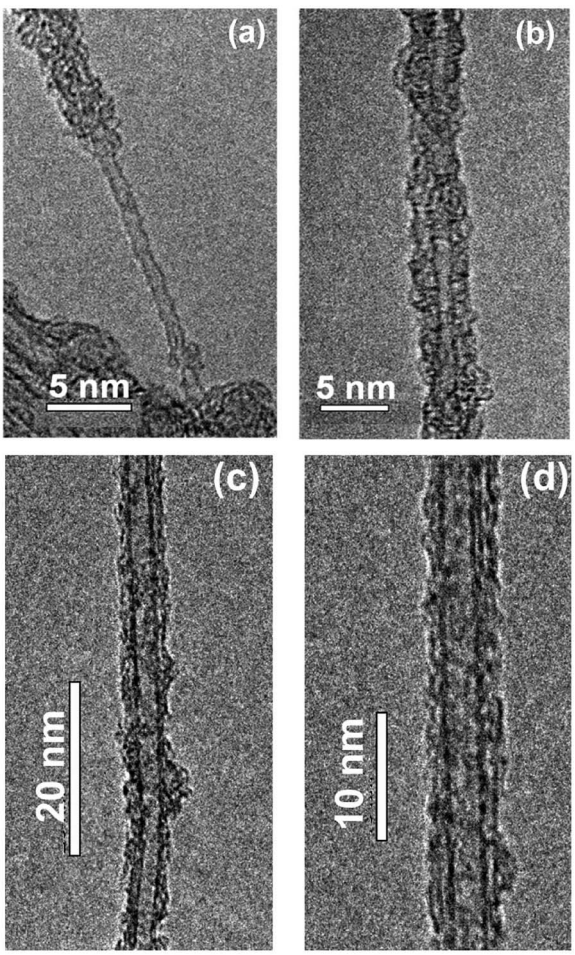
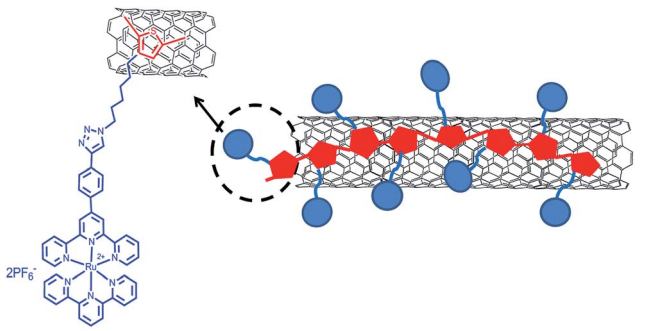


Fig. 4 TEM images of SWCNTs functionalized with polymer **5**. (a) and (b) show SWCNTs with a diameter of *ca.* 1.0 nm; (c) and (d) show SWCNTs with a larger diameter (*ca.* 1.5–2.0 nm).

Transient absorption spectroscopy and electron transfer kinetics

The photophysical properties of the hybrid formed between polymer **5** and SWCNTs were studied by fs-TA spectroscopy. For comparison purpose, the fs-TA spectra of complex **4** and polymer **2** were also collected (Fig. S6 and S7†). After photoexcitation of complex **4**, a singlet ^{1}MLCT excited state[40] [Ru(π)t_{2g} to ^{1}tpy(π*)] was generated and it underwent a very fast intersystem crossing (ISC) within the instrument response time ($\tau \leq 150$ fs) to the triplet ^{3}MLCT (Ru–^{3}tpy$_2$) excited state.[41,42] Therefore, the initial species formed exhibits a broad transient absorption band at 620 nm at 1 ps (Fig. S6a†), which is assigned to the ^{3}MLCT excited state of complex **4**. The negative band at 490 nm is attributed to the bleaching of the ground state (see Fig. 1a). Subsequently, a torsional relaxation of the excited state species to a more planar structure between the phenylene ring and the



Scheme 2 Schematic illustration of SWCNTs functionalized with polymer **5**.

 This journal is © The Royal Society of Chemistry 2017

Published on 17 August 2017. Downloaded by Rice University on 11/17/2023 5:06:50 PM.

terpyridine ligand takes places in 7 ps,[43] which is similar to the results obtained in our previous study on Ru(II) terpyridine thiocyanate complexes.[44] After 33.6 ps, the bands at 490 and 617 nm decay (Fig. S6b†) with a time constant of 1 ns, which is due to the decay of the ^{3}MLCT excited states.[40] For the metal free polymer **2**, its fs-TA spectra are shown in Fig. S7.† The strong negative band at 460 nm is assigned to bleaching of the ground state and the band at 570 nm is due to the stimulated emission of the polymer backbone.[31]

The fs-TA spectra of polymer **5** in DMF at different stages are shown in Fig. 5a and b. Unlike complex **4**, the bleaching band at 490 nm shows an asymmetrical narrowing from 0.8 to 3 ps with a decrease in intensity, while the intensity of the band at *ca.* 600 nm increases. With reference to the absorption and emission spectra (Fig. 1), this is assigned to the formation of a charge separated state by an electron transfer from the polythiophene singlet excited state to Ru(II) within 1.2 ps.[31] Subsequently, the Ru complex ^{1}MLCT excited states undergo a rapid ISC process to the ^{3}MLCT excited states within the instrument response time ($\tau < 150$ fs), resulting in an absorption band at 680 nm. The peak position shows a red shift compared to that observed in complex **4**. This may be due to the lower ^{3}MLCT excited state energy after the formation of a triazole unit next to the terpyridine ligand. The torsional relaxation process that occurred at the triplet Ru(II) complex leads to the changes in the spectra observed from 3 to 30 ps. Therefore, fitting of the decay of the band at 680 nm (Fig. 5c inset) yields two time constants ($\tau_1 =$ 7.7 ps and $\tau_2 = 1.2$ ns). The fast process is due to the torsional relaxation processes, while the slower one is due to the decay of the ^{3}MLCT species. At 2.82 ns, the TA spectrum shows a weak absorption at 550 nm, which is assigned to the formation of a charge separated state, and is consistent with observations made in other similar systems.[31]

After the formation of the polymer **5**/SWCNT hybrid, there are changes in the photophysical properties due to the strong electronic interaction between the Ru(II) complexes and the polythiophene/SWCNTs. Fig. 6a and b show the fs-TA spectra of polymer **5**/SWCNT hybrid dispersion in DMF. The asymmetric

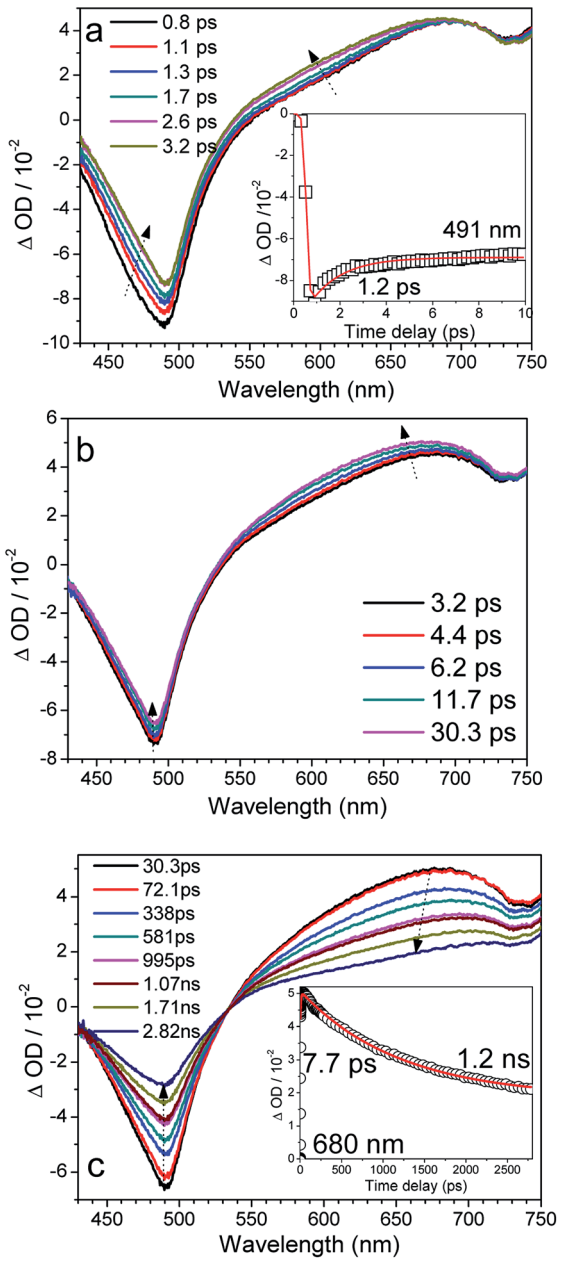


Fig. 5 (a–c) fs-TA spectra of polymer **5** in DMF achieved after 400 nm excitation. The kinetics of the decay processes at 491 nm and 680 nm are shown as inset diagrams (in a and c).

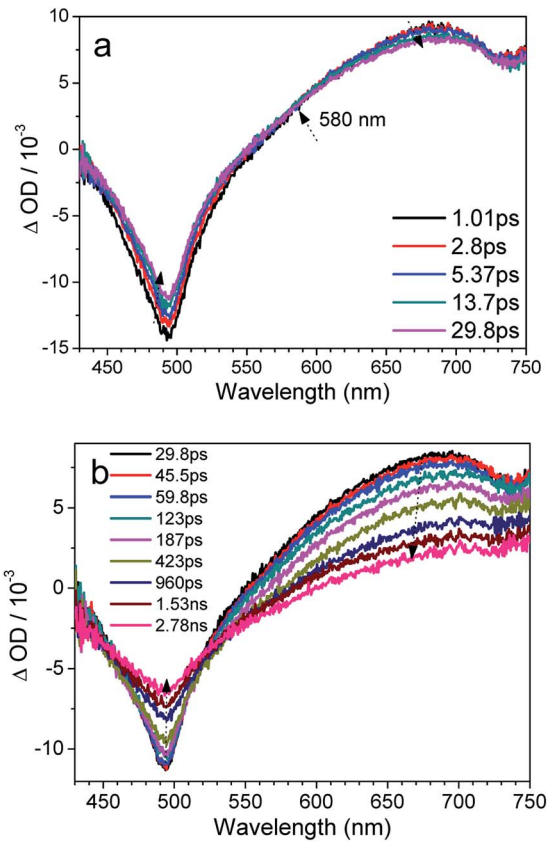


Fig. 6 (a, b) fs-TA spectra of the polymer **5**/SWCNT hybrid in DMF (excited at 400 nm).

Published on 17 August 2017. Downloaded by Rice University on 11/17/2023 5:06:50 PM.

narrowing of the bleaching band is negligible in the early delay time (Fig. 6a), which suggests that the energy transfer process between the polythiophene backbone and Ru(II) complexes could be inhibited due to the strong electronic interaction between the polythiophene and SWCNTs. The effect of SWCNTs on the excited state properties of polymer **5** was further examined by analysing their spectra using a global fitting, and these results are shown in Fig. S8 and S9.† For the pure polymer **5**, it was examined by both Decay Associated Difference Spectra (DADS) and Evolution Associated Difference Spectra (EADS) models.[45] Since the Ru(II) complex undergoes two independent (and parallel) photophysical processes, the DADS results should be more appropriate for interpretation (Fig. S8a†). The time constants determined from global fitting are 3.4 ps and 1.25 ns. The second time constant is consistent with the results observed in Fig. 5 and is due to the decay of the triplet excited state of the Ru complex. Another long lived species was also observed, but its decay time could not be measured by the global fitting. Such a long-lived species is likely due to the previously reported charge separated excited state (lifetime > 20 μs).[31] The asymmetric narrowing of the bleaching band at 490 nm and the decay of the stimulated fluorescence band at *ca.* 580 nm are assigned to the charge separation process as discussed above. For the polymer **5**/SWCNT hybrid, the sequential EADS model was adopted (Fig. S9†), from which 3 time constants (0.4 ps, 167 ps and 4.7 ns) were obtained. The EADS at 0.4 ps is due to the torsional relaxation of the polymer **5** ^{3}*MLCT excited state as discussed above. The subsequent broad band observed (second EADS) is recognized as the polymer **5** ^{3}MLCT excited state, leading to the formation of the charge-separated state polymer $\mathbf{5}^{\bullet+}$/SWCNT$^{\bullet-}$ in 167 ps.[44] The longer decay process (4.7 ns) is assigned to the charge recombination process. Since the lifetime of such a long-lived species was not observed in polymer **5**, those observed in the TA spectra of polymer **5**/SWCNTs could not be due to the charge separated species resulting from a charge transfer from the polythiophene backbone to the Ru(II) complex. This can also be seen by the difference in the global fitting results for the long-lived species observed in polymer **5** and polymer **5**/SWCNTs (Fig. S10†). If the electron transfer is indeed the only process after photoexcitation, there should be no change in the bleaching band of the Ru(II) complex. However, in this case, a small difference in the intensities of the bleaching bands between the second and the third EADS spectra is observed. This is suggested to be due to the partial detachment of polymer segments from the SWCNT surface after excitation by the laser pulses. Nevertheless, the significant change in the decay time constant (from 1.2 ns to 167 ps) of polymer **5** ^{3}MLCT excited states suggests that an electron injection from polymer **5** to SWCNTs is a more plausible mechanism.

Based on the experimental results obtained, a schematic diagram showing the energetic and kinetic data of all these processes is summarized in Fig. 7. The TA results strongly suggest a fast electron injection process in this photosensitizer-SWCNT system. Since the photophysical properties of these carbon nanotube-based donor–acceptor hybrids are strongly dependent on the electronic properties of the nanotube (and its diameter) as well as the nature of the excited states of the photosensitizing metal complex, by performing ultrafast time-resolved transient absorption spectroscopy, it is possible to study the details of the electron flow process, and to construct new and efficient light harvesting systems by choosing an appropriate pair of sensitizer/electron acceptors.

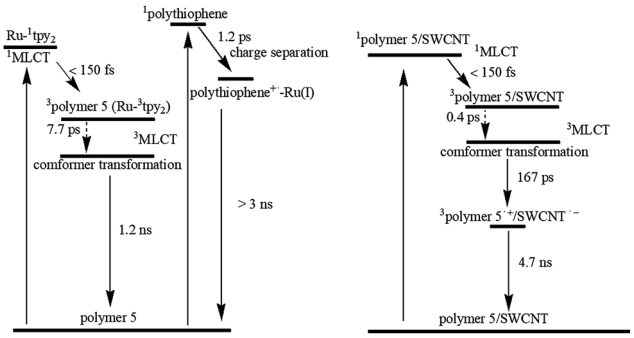


Fig. 7 Schematic diagram showing the photophysical processes in polymer **5** (left) and the charge injection process in the polymer **5**/SWCNT hybrid (right).

Conclusions

A regioregular polythiophene incorporated with photosensitizing ruthenium complexes at the side chains was synthesized. The polymer showed a strong interaction with SWCNTs with a diameter of 0.9 to 2.0 nm, and could form stable dispersion with SWCNTs in polar solvents. Raman spectroscopic results showed that SWCNTs with specific diameters could be dispersed. Transmission electron microscopic images revealed that SWCNTs with both small and large diameters can be functionalized with the polymer. Ultrafast transient absorption spectroscopy revealed a fast electron transfer process from the sensitizing Ru(II) complex to SWCNTs with a time constant of 167 ps. The present study demonstrated the selective dispersion of SWCNTs by this functional conjugated polymer, and the evidence of electron injection from the sensitizers to SWCNTs. The system presented may serve as a model for the design of new light harvesting systems based on polymer/SWCNT hybrids. It should be noted that the model presented here is a simplified description of the photophysics in a complex disordered system which cannot be analysed in more detail at this stage due to limitations of the instrumentation and the properties of the excited species involved.

Experimental methods

Complex 4

In a nitrogen purged, reflux condenser equipped flask, 2,2′:6′,2″-terpyridine (160 mg, 0.687 mmol), ruthenium trichloride (216 mg, 0.824 mmol) and methanol were added. The mixture was heated to reflux for 5 h and the solid was collected by filtration. The obtained product 2,2′:6′,2″-terpyridine ruthenium chloride [Ru(tpy)Cl$_3$] (260 mg, 0.587 mmol) was added in ethylene glycol (20 ml) with (4-ethynylphenyl)-2,2′:6′,2″-

 This journal is © The Royal Society of Chemistry 2017

Published on 17 August 2017. Downloaded by Rice University on 11/17/2023 5:06:50 PM.

terpyridine (195 mg, 0.587 mmol) together in a flask. Several drops of *N*-ethylmorpholine were added and then the reaction solution was stirred at 100 °C for 2 h. The mixture was allowed to cool, and then poured into water (75 ml). A saturated aqueous solution of KPF_6 (1 ml) was added and the precipitate was collected by filtration. The obtained solid was purified by silica gel column chromatography using MeCN : saturated aqueous KNO_3 : H_2O (20 : 2 : 1) mixtures as the eluent. The complex **4** was collected as a red solid (150 mg, yield: 28%). ^{1}H NMR (400 MHz, CD_3CN) δ (ppm): 9.02 (s, 2H), 8.76 (d, 2H), 8.64 (d, 2H), 8.50 (d, 2H), 8.42 (m, 1H), 8.21 (d, 2H) 7.94–7.87 (m, 6H), 7.41 (d, 2H), 7.35 (d, 2H), 7.18–7.15 (m, 4H), 3.67 (s, 1H). ^{13}C NMR (100 MHz, CD_3CN) δ (ppm): 159.06, 156.6, 156.4, 153.6, 153.4, 148.2, 139.12, 139.07, 138.2, 136.9, 134.1, 129.0, 128.54, 128.48, 125.6, 125.4, 125.0, 124.8, 122.6, 83.7, 81.3. MS: *m*/*z* 812.8 ($M - PF_6$), 667.9 ($M - 2PF_6$).

Polymer 2

2,5-Dibromo-3-(6-bromohexyl)thiophene (600 mg, 1.48 mmol) was dissolved in try THF (15 ml), and the solution was cooled to 0 °C under a nitrogen atmosphere. i-PrMgCl·LiCl solution (1.3 M in THF, 1.4 ml) was added and the mixture was stirred for 30 min at 0 °C. Then Ni(dppp)Cl_2 (5 mg, 0.009 mmol) was added to initiate the polymerization. The reaction was stirred at 40 °C for 2 h and then at 25 °C for another 8 h. The polymer was precipitated into a HCl/MeOH mixture, and the solid obtained was purified with methanol and *n*-hexane by Soxhlet extraction (24 h for each solvent). The polymer was then dissolved in chloroform and precipitated in methanol. After filtration, the polymer was obtained as a dark red solid (181 mg, yield: 50%). ^{1}H NMR (400 MHz, $CDCl_3$) δ (ppm): (6.97 s, 1H), 3.44 (t, 2H), 2.82 (t, 2H), 1.94 (m, 2H), 1.84 (m, 2H), 1.49 (m, 4H).

Polymer 3

Sodium azide (52 mg) and 18-crown-6 (310 mg) were added to DMF (8 ml), and the mixture was sonicated until a homogeneous solution was obtained. The solution was then added to a solution of polymer **2** (20 mg) in THF (24 ml) under a nitrogen atmosphere. The mixture was heated at 40 °C for 8 h. After removing THF with a rotary evaporator, the solution left was added to methanol (100 ml). The precipitate was collected by vacuum filtration, and the product was obtained as a black solid (16 mg, yield: 94%). Due to the reactivity of the azide group, the freshly prepared polymer 3 was used immediately for the next step. ^{1}H NMR (400 MHz, $CDCl_3$) δ (ppm): (6.97 s, 1H), 3.29 (t, 2H), 2.82 (t, 2H), 1.74–1.46 (m, 8H).

Polymer 5

Polymer **3** (10 mg, 0.048 mmol), complex **4** (62 mg, 0.065 mmol), PMDETA (11 mg, 0.065 mmol), sodium ascorbate (6 mg, 0.03 mmol), THF (12 ml), and DMF (5 ml) were mixed in a round bottom flask. The solution was degassed by bubbling with nitrogen gas for 30 min. CuBr (9 mg, 0.07 mmol) was added to the mixture, and the solution was further degassed by bubbling with nitrogen gas for another 20 min. The solution was stirred at room temperature for 48 h in the dark in a nitrogen atmosphere. Then under nitrogen purging, additional degassed DMF solution (3 ml) of complex **4** (32 mg, 0.033 mmol), PMDETA (6 mg, 0.03 mmol), sodium ascorbate (3 mg, 0.02 mmol) and CuBr (5 mg, 0.03 mmol) was added to the reaction mixture, and the solution was stirred at 40 °C for another 24 h. THF in the solution was removed using a rotary evaporator, and the solution was poured into methanol (100 ml). Saturated aqueous KPF_6 solution (1 ml) was added to the solution, and the precipitate was collected by filtration. The product was obtained as a dark red solid (50 mg, yield: 89%).^{1}H NMR (400 MHz, DMSO) δ (ppm): 8.99 (bs, 2H), 8.73–8.57 (m, 4H), 8.49–8.37 (m, 3H), 8.29–8.10 (m, 5H), 7.89 (bs, 4H), 7.45 (bs, 2H), 7.36 (bs, 2H), 7.15–6.99 (m, 5H), 4.31 (bs, 2H), 2.81 (bs, 2H), 1.90–1.40 (m, 8H).

Functionalization of carbon nanotubes

SWCNTs (1 mg) were added to a solution of polymer **5** (5 mg) in DMF (10 ml). The mixture was sonicated for 1 h. After cooling in an ice bath, the solution was centrifuged at 10 000 rpm for 20 min. The supernatant was collected and filtered with a PTFE membrane filter (pore size = 0.1 μm). The excess polymer was removed by washing with DMF. The washing process was repeated until there was no polymer present in the solvent, as monitored by UV-Vis absorption spectroscopy. The polymer/SWCNT hybrid on the membrane surface was redispersed in DMF.

fs-TA spectroscopic experiment

The spectroscopic measurements were conducted according to a previously reported procedure. The details are described in the ESI.†[46,47]

Conflicts of interest

There are no conflicts to declare.

Acknowledgements

The work described in this paper was supported by the Research Grants Council of the Hong Kong Special Administrative Region, China (Project No. HKU700613E, AoE/P-03/08). Partial financial support from the Hong Kong UGC Special Equipment Grants (SEG HKU07) and the University Development Fund (U of HK) project on "New Ultrafast Spectroscopy Experiments for Shared Facilities" is also acknowledged.

Notes and references

1 P. Avouris, Z. H. Chen and V. Perebeinos, *Nat. Nanotechnol.*, 2007, **2**, 605–615.
2 P. Avouris, M. Freitag and V. Perebeinos, *Nat. Photonics*, 2008, **2**, 341–350.
3 X. Li, Y. Jia, J. Wei, H. Zhu, K. Wang, D. Wu and A. Cao, *ACS Nano*, 2010, **4**, 2142–2148.
4 H. Wang, J. Mei, P. Liu, K. Schmidt, G. Jimenez-Oses, S. Osuna, L. Fang, C. J. Tassone, A. P. Zoombelt,

Published on 17 August 2017. Downloaded by Rice University on 11/17/2023 5:06:50 PM.

A. N. Sokolov, K. N. Houk, M. F. Toney and Z. Bao, *ACS Nano*, 2013, **7**, 2659–2668.
5 J. P. Bourgoin, S. Campidelli, P. Chenevier, V. Derycke, A. Filoramo and M. F. Goffman, *Chimia*, 2010, **64**, 414–420.
6 F. D'Souza and O. Ito, *Chem. Commun.*, 2009, **33**, 4913–4928.
7 E. Maligaspe, A. S. D. Sandanayaka, T. Hasobe, O. Ito and F. D'Souza, *J. Am. Chem. Soc.*, 2010, **132**, 8158–8164.
8 A. S. Sandanayaka, N. K. Subbaiyan, S. K. Das, R. Chitta, E. Maligaspe, T. Hasobe, O. Ito and F. D'Souza, *ChemPhysChem*, 2011, **12**, 2266–2273.
9 F. D'Souza, S. K. Das, M. E. Zandler, A. S. Sandanayaka and O. Ito, *J. Am. Chem. Soc.*, 2011, **133**, 19922–19930.
10 D. M. Guldi, G. M. Rahman, N. Jux, D. Balbinot, U. Hartnagel, N. Tagmatarchis and M. Prato, *J. Am. Chem. Soc.*, 2005, **127**, 9830–9838.
11 G. Mountrichas, A. S. D. Sandanayaka, S. P. Economopoulos, S. Pispas, O. Ito, T. Hasobe and N. Tagmatarchis, *J. Mater. Chem.*, 2009, **19**, 8990–8998.
12 D. M. Guldi, G. M. Rahman, V. Sgobba, N. A. Kotov, D. Bonifazi and M. Prato, *J. Am. Chem. Soc.*, 2006, **128**, 2315–2323.
13 L. Hu, Y. L. Zhao, K. Ryu, C. Zhou, J. F. Stoddart and G. Gruner, *Adv. Mater.*, 2008, **20**, 939–946.
14 A. Vijayaraghavan, *J. Mater. Chem.*, 2012, **22**, 7083–7087.
15 G. J. Brady, Y. Joo, M. Y. Wu, M. J. Shea, P. Gopalan and M. S. Arnold, *ACS Nano*, 2014, **8**, 11614–11621.
16 W. Xu, J. Zhao, L. Qian, X. Han, L. Wu, W. Wu, M. Song, L. Zhou, W. Su, C. Wang, S. Nie and Z. Cui, *Nanoscale*, 2014, **6**, 1589–1595.
17 W. Y. Tam, C. S. K. Mak, A. M. C. Ng, A. B. Djurisic and W. K. Chan, *Macromol. Rapid Commun.*, 2009, **30**, 622–626.
18 C. H. Li, M. C. N. Alan, C. S. K. Mak, A. B. Djurisic and W. K. Chan, *ACS Appl. Mater. Interfaces*, 2012, **4**, 74–80.
19 A. Hagfeldt, G. Boschloo, L. Sun, L. Kloo and H. Pettersson, *Chem. Rev.*, 2010, **110**, 6595–6663.
20 J. T. Hyde, K. Hanson, A. K. Vannucci, A. M. Lapides, L. Alibabaei, M. R. Norris, T. J. Meyer and D. P. Harrison, *ACS Appl. Mater. Interfaces*, 2015, **7**, 9554–9562.
21 P. Imin, F. Y. Cheng and A. Adronov, *Polym. Chem.*, 2011, **2**, 411–416.
22 H. Gu and T. M. Swager, *Adv. Mater.*, 2008, **20**, 4433–4437.
23 H. W. Lee, Y. Yoon, S. Park, J. H. Oh, S. Hong, L. S. Liyanage, H. Wang, S. Morishita, N. Patil, Y. J. Park, J. J. Park, A. Spakowitz, G. Galli, F. Gygi, P. H. Wong, J. B. Tok, J. M. Kim and Z. Bao, *Nat. Commun.*, 2011, **2**, 541.
24 S. K. Samanta, M. Fritsch, U. Scherf, W. Gomulya, S. Z. Bisri and M. A. Loi, *Acc. Chem. Res.*, 2014, **47**, 2446–2456.
25 E. Puodziukynaite, L. Wang, K. S. Schanze, J. M. Papanikolas and J. R. Reynolds, *Polym. Chem.*, 2014, **5**, 2363–2369.
26 J. M. Lobez and A. Afzali, *Chem. Mater.*, 2013, **25**, 3662–3666.
27 L. Zhai, R. L. Pilston, K. L. Zaiger, K. K. Stokes and R. D. McCullough, *Macromolecules*, 2003, **36**, 61–64.
28 D. Lee and D. J. Jang, *Polymer*, 2014, **55**, 5469–5476.
29 J. P. Sauvage, J. P. Collin, J. C. Chambron, S. Guillerez, C. Coudret, V. Balzani, F. Barigelletti, L. De Cola and L. Flamigni, *Chem. Rev.*, 1994, **94**, 993–1019.
30 J. T. Hewitt, P. J. Vallett and N. H. Damrauer, *J. Phys. Chem. A*, 2012, **116**, 11536–11547.
31 L. Wang, E. Puodziukynaite, E. M. Grumstrup, A. C. Brown, S. Keinan, K. S. Schanze, J. R. Reynolds and J. M. Papanikolas, Polymer, *J. Phys. Chem. Lett.*, 2013, **4**, 2269–2273.
32 A. Keerthi and S. Valiyaveettil, *J. Phys. Chem. B*, 2012, **116**, 4603–4614.
33 Y. Tanaka, Y. Hirana, Y. Niidome, K. Kato, S. Saito and N. Nakashima, *Angew. Chem., Int. Ed.*, 2009, **48**, 7655–7659.
34 A. M. Rao, E. Richter, S. Bandow, B. Chase, P. C. Eklund, K. A. Williams, S. Fang, K. R. Subbaswamy, M. Menon, A. Thess, R. E. Smalley, G. Dresselhaus and M. S. Dresselhaus, *Science*, 1997, **275**, 187–191.
35 A. M. Rao, P. C. Eklund, S. Bandow, A. Thess and R. E. Smalley, *Nature*, 1997, **388**, 257–259.
36 J. H. Zou, L. W. Liu, H. Chen, S. I. Khondaker, R. D. McCullough, Q. Huo and L. Zhai, *Adv. Mater.*, 2008, **20**, 2055–2060.
37 F. Hennrich, R. Krupke, S. Lebedkin, K. Arnold, R. Fischer, D. E. Resasco and M. M. Kappes, *J. Phys. Chem. B*, 2005, **109**, 10567–10573.
38 S. M. Bachilo, M. S. Strano, C. Kittrell, R. H. Hauge, R. E. Smalley and R. B. Weisman, *Science*, 2002, **298**, 2361–2366.
39 M. Khadem and Y. Zhao, *J. Org. Chem.*, 2015, **80**, 7419–7429.
40 M. Maestri, N. Armaroli, V. Balzani and E. C. Constable, *Inorg. Chem.*, 1995, **34**, 2759–2767.
41 A. C. Bhasikuttan, M. Suzuki, S. Nakashima and T. Okada, *J. Am. Chem. Soc.*, 2002, **124**, 8398–8405.
42 Q. C. Sun, S. Mosquera-Vazquez, Y. Suffren, J. Hankache, N. Amstutz, L. M. L. Daku, E. Vauthey and A. Hauser, *Coord. Chem. Rev.*, 2015, **282**, 87–99.
43 N. H. Damrauer and J. K. McCusker, *J. Phys. Chem. A*, 1999, **103**, 8440–8446.
44 H. Shi, L. Du, K. Lo, W. Xiong, W. K. Chan and D. L. Phillips, *J. Phys. Chem. C*, 2017, **121**, 8145–8152.
45 I. H. M. van Stokkum, D. S. Larsen and R. van Grondelle, *Biochim. Biophys. Acta*, 2004, **1657**, 82–104.
46 L. Du, M. D. Li, Y. Zhang, J. Xue, X. Zhang, R. Zhu, S. C. Cheng, X. Li and D. L. Phillips, *J. Org. Chem.*, 2015, **80**, 7340–7350.
47 L. Du, W. Xiong, S. C. Cheng, H. Shi, W. K. Chan and D. L. Phillips, *J. Phys. Chem. Lett.*, 2017, **8**, 2475–2479.

 This journal is © The Royal Society of Chemistry 2017